Nanoscale

Accepted Manuscript

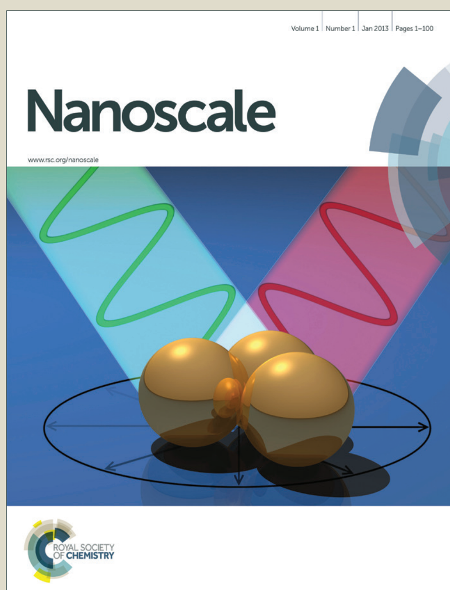

This is an *Accepted Manuscript*, which has been through the Royal Society of Chemistry peer review process and has been accepted for publication.

Accepted Manuscripts are published online shortly after acceptance, before technical editing, formatting and proof reading. Using this free service, authors can make their results available to the community, in citable form, before we publish the edited article. We will replace this *Accepted Manuscript* with the edited and formatted *Advance Article* as soon as it is available.

You can find more information about *Accepted Manuscripts* in the Information for Authors.

Please note that technical editing may introduce minor changes to the text and/or graphics, which may alter content. The journal's standard Terms & Conditions and the Ethical guidelines still apply. In no event shall the Royal Society of Chemistry be held responsible for any errors or omissions in this *Accepted Manuscript* or any consequences arising from the use of any information it contains.

ROYAL SOCIETY OF CHEMISTRY

www.rsc.org/nanoscale

Electrical Breakdown of Multilayer MoS_2 Field-Effect Transistors with Thickness-Dependent Mobility

Rui Yang[1], Zenghui Wang[1], Philip X.-L. Feng[1,*]

[1]*Department of Electrical Engineering & Computer Science, Case School of Engineering*
Case Western Reserve University, 10900 Euclid Avenue, Cleveland, OH 44106, USA

We report on experimental investigation and modeling of electrical breakdown in multilayer (few- to tens-of-nanometer-thick) molybdenum disulfide (MoS_2) field-effect transistors (FETs). By measuring MoS_2 devices ranging from 5.7nm to 77nm in thicknesses, we achieve breakdown current of 1.2mA, mobility of 42 $cm^2V^{-1}s^{-1}$, and on/off current ratio I_{On}/I_{Off}~10^7. Through measurement and simulation, we find the dependence of breakdown current limit on MoS_2 thicknesses, channel lengths and conductivities. We also explore, both experimentally and analytically, the effects of different device parameters upon carrier mobility, which is directly related to the current carrying capacity. The results suggest that, compared to single-layer devices, multilayer MoS_2 FETs could be advantageous for circuit applications requiring higher carrier mobility and power handling capacities.

Nanoscale Accepted Manuscript

*Corresponding Author. Email: philip.feng@case.edu

Ultrathin molybdenum disulfide (MoS_2) isolated from its layered bulk material has recently emerged as a new two-dimensional (2D) semiconducting crystal with a wide spectrum of attractive properties – such as lack of dangling bonds, high thermal stability, and thickness-dependent bandgap and bandstructure[1,2]. These lead to strong promises for creating new nanodevices beyond graphene[3], ranging from ultrathin field effect transistors (FETs) and optoelectronic devices to 2D sensors and transducers, on both rigid and flexible substrates. While prototype single- and few-layer MoS_2 FETs[4,5,6,7,8,9,10,11], circuits[12,13,14] and memory devices[15] have been demonstrated, multilayer (up to tens of nanometers thick) devices[16,17,18,19,20,21,22,23,24] are more desirable for certain applications: they are expected to have higher carrier mobility and density of states under the same dielectric environment, higher current limit, and better manufacturability, while occupying similar device footprint as their single- and few-layer counterparts. To date, flexible electronics[25,26] and gas sensors[27] based on multilayer MoS_2 FETs, and a small-signal generator based on multilayer MoS_2/graphene heterojunction[28] have already been reported.

The maximum current and current density of a transistor determine the power it can handle, which is important for designing integrated circuit[29]. While initial exploration of electrical breakdown in single-layer MoS_2 transistors has been reported[30], current limit in multilayer devices remains to be investigated. A number of device parameters can affect this limit, such as dimensions and conductivity of the transistor channel. A highly conductive channel is desirable, as it leads to less Joule heating under a given electric current. This further leads to the open challenge of obtaining high electron mobility in MoS_2 transistors.

Nanoscale Accepted Manuscript

The mobility of MoS_2 transistors has been studied for a variety of device structures[1-3]. At room temperature, measured single-layer MoS_2 transistors on the substrate show mobility of 60 $cm^2V^{-1}s^{-1}$ in vacuum[31], much less than the theoretical optical-phonon-scattering-limited mobility (410 $cm^2V^{-1}s^{-1}$)[32]. To approach high mobility, high-κ dielectric materials (*e.g.*, HfO_2, Al_2O_3) have been adopted to build top-gated devices[4,5,13,14,17]. It has also been recently noted that some of the reported mobility values from top-gated devices may have been overestimated[33]. In contrast, multilayer MoS_2 transistors (a few to tens of nanometer thick)[34] with relatively simple back-gated configuration exhibit mobility values up to 470 $cm^2V^{-1}s^{-1}$ at room temperature[22] on PMMA substrate, close to the theoretically predicted phonon scattering limit (200-500 $cm^2V^{-1}s^{-1}$) for bulk molybdenum disulfide[4].

To further understand and utilize the unique properties offered by multilayer MoS_2 transistors (a few to tens-of-nanometers thick), we investigate device characteristics such as electrical breakdown limit and electron mobility, focusing on their dependence on device parameters such as MoS_2 thickness. Through a series of experimental measurements, analytical calculations, and finite element modeling (FEM), we find that to achieve higher electrical breakdown limit, higher device thickness and channel conductivity are desired. We further examine the difference between single-layer and multilayer devices, and illustrate how heat dissipation and current carrying capabilities scale with layer numbers in MoS_2 FETs with different device configurations. Multilayer devices can achieve higher mobility and higher current limit than mono- or few-layer MoS_2 FETs, and thus can be better suited for certain circuit applications.

The multilayer MoS_2 devices are fabricated by mechanically exfoliating MoS_2 crystal onto 290nm-thick SiO_2 on Si substrate and patterning electrical contacts using electron-beam lithography (EBL). Contacts are then metallized using electron-beam evaporation followed by

Nanoscale Accepted Manuscript

lift-off. Figure 1(a) shows the schematic of our MoS_2 transistors and their electrode configurations. During measurement the electrodes are connected to high-precision source measurement units (SMUs) which supply the voltages and measure the currents. During measurement SMU1 is connected to the back gate (G) and SMU2 is connected to the drain (D). The source (S) electrode is grounded. The thicknesses of the MoS_2 layers are measured using an atomic force microscope (AFM). Figures 1(b)-1(d) illustrate the band diagrams of multilayer MoS_2 transistors under different operation conditions. Ti (Titanium) forms Schottky contact to MoS_2 with a barrier height $q\phi_B = q\psi_M - \chi$, where $q\psi_M$ is the work function of the contact metal and χ is the electron affinity of MoS_2. While the estimated Schottky barrier height for Ti to MoS_2 is ~0.3eV, in practice $q\Phi_B$ is lowered to around 50meV due to Fermi level pinning[18]. This suggests that at room temperature, thermally assisted tunneling is the dominant conduction mechanism at ON state (compared to thermionic emission, Fig. 1 (d)). When a back gate voltage V_G higher than the threshold voltage V_T is applied, the Fermi level E_F of MoS_2 moves closer to the conduction band, narrowing the width of the Schottky barrier, and facilitating thermally assisted tunneling between the D and S electrodes[7]. In contrast, if $V_G<V_T$, E_F moves away from the conduction band, widening the Schottky barrier, thus suppressing tunneling (the OFF state).

Figure 2 shows characterization of two multilayer MoS_2 transistors (devices A&B) with Ti/Ni contacts. For device A (thickness $t\approx 70$nm), current saturation is observed under large positive drain bias V_D (Fig. 2(b)), desirable for field effect transistors. At positive V_G, the device turns on, and conductance increases with V_G, confirming n-type transistor behavior (Figs. 2(c)-2(d)). The off state leakage current I_{Off} is ~ 100pA, much smaller than the on-state current I_{On}, showing an on/off ratio (I_{On}/I_{Off}) of ~10^4. From data in Fig. 2(c) we extract the field-effect mobility $\mu=(dI_D/dV_G)\times[L/(WC_{ox}V_D)]$, where L, W, C_{ox} are respectively the length, width, and the

Nanoscale Accepted Manuscript

capacitance per unit area to the back gate of the MoS_2 channel. For device A, μ=42 $cm^2V^{-1}s^{-1}$, comparable with other reported devices with similar structure[16,20,21,23]. For device B (Figs. 2(e)-2(h)), a much thinner device (t=5.7nm) also with Ti/Ni contact, we find μ=9.9 $cm^2V^{-1}s^{-1}$ and $I_{On}/I_{Off}=4\times10^6$, again consistent with similar devices[19,20,21,22,23].

Figure 3 summarizes μ and I_{On}/I_{Off} of 10 devices with different thicknesses and contact materials (also shown in Table S1). We observe that thicker MoS_2 transistors in general exhibit higher mobilities (Fig. 3(a)), consistent with literature[18,19,21]. We model the μ–t relation using Boltzmann transport equation[32]. We consider scattering from phonon, charged impurity, boundary, lattice defects, and thickness steps, with phonon scattering including contributions from acoustic, polar optical (POP), and homopolar optical (HOP) phonons (effect from surface optical phonon is expected to be negligible in our devices with SiO_2 gate dielectric[35]). To date, only phonon and impurity scatterings have been analyzed for MoS_2 FETs[32,35,36], as the other mechanisms were deemed negligible for single layer devices, which does not necessarily hold for multilayer devices. All these mechanisms have different scattering strengths and thickness dependence. Among them, phonon is the most common scattering source at room temperature, and is expected to be independent of MoS_2 thickness[19,32,35,37]. Charged impurity scattering is also important, and is thickness dependent[36]. Electron-boundary, generating less scattering than charged impurity, is also thickness dependent[38]. Lattice vacancy is the most common (and a native) defect in MoS_2[39], and vacancy scattering does not depend on thickness. The calculated vacancy scattering rate is comparable with other scattering mechanisms[40]. We also include scattering due to thickness steps created in the mechanical exfoliation process, and find it also important[41].

Nanoscale Accepted Manuscript

Combining contributions from all the mechanisms above, we calculate the total scattering rate $(\tau_{total})^{-1}$ using the empirical expression: $\frac{1}{\tau_{total}} = \frac{1}{\tau_{phonon}} + \beta\frac{1}{\tau_{imp}} + \frac{1}{\tau_{bdr}} + \frac{1}{\tau_{va}} + \frac{1}{\tau_{step}}$, where the 5 terms represent contribution from phonon, impurity, boundary, vacancy, and step, respectively, with the phonon term further consists of multiple mechanisms: $\frac{1}{\tau_{phonon}} = \frac{1}{\tau_{acoustic}} + \frac{1}{\tau_{POP}} + \frac{1}{\tau_{HOP}}$, and β is an empirical fitting parameter (see Supplementary Information for details). We find that at small thickness, charged impurity scattering is the main scattering mechanism, and at larger thickness vacancy scattering and thickness step scattering become dominant. Mobility calculated from this model $\mu_n = \frac{q\tau_{total}}{m^*}$ (q: elementary charge, m^*: electron effective mass) shows good agreement with our data, with thicker devices exhibiting higher mobilities (Fig. 3(a)). Fig. 3(b) shows that typically thinner devices have higher I_{On}/I_{Off}. Our results illustrate the tradeoff between mobility and on/off ratio in MoS_2 devices, suggesting that choosing proper device thickness can be helpful for achieving the desired performance.

While mobility and on/off ratio are important device parameters for logical circuits, the current carrying limit is critical for applications requiring high current/power. Here, we study electrical breakdown in multilayer MoS_2 devices with different thicknesses (Fig. 4). All the measured devices have 50nm Ni (Nickel) contact, and we perform annealing in N_2 at 350°C in vacuum (1 Torr) to improve the MoS_2-metal contact. We first calibrate the transfer characteristic of the devices, and then perform transport measurement at V_G≈50V to turn on the device, and gradually increase the range of drain voltage sweeps. As shown in Fig. 4(a), a ~70nm-thick MoS_2 device breaks down when V_D is swept from 0 to 30V for the second time, at the breakdown current I_{BD}=1.2mA. This is among the highest current values reported to date for

Nanoscale Accepted Manuscript

MoS_2 transistors, corresponding to a breakdown current density J_{BD}=4.9×10^9A/m^2 (device width W=3.5μm). In three other devices tested (Fig. 4(b)-(d)), we observe discrete decreases in device conductance after each V_D sweep (Figs. 4(b)-4(d) inset). This is consistent with Joule-heating-induced oxidation which has been observed in graphene nanoribbons[29].

We find that thicker devices exhibit higher breakdown current limit than thinner devices. This suggests that multilayer MoS_2 FETs are advantageous compared to single-layer devices by carrying more power while having the same device footprint. We also compare the normalized "per-layer" current-carrying capability between single-layer and multilayer devices. We find that higher "per-layer" current limit (1.18×10^6 A/m) has been reported for single-layer MoS_2 FET[30] than for the multilayer devices we measure here (1.76×10^4 A/m). Besides difference in detailed device structure and parameters, the decrease in "per-layer" current limit is in fact intrinsic to multilayer devices with regular device geometries due to two main reasons, both of which have important implications for designing high-performance devices. First, for devices with conventional, 2D surface contacts, the contact area remains roughly unchanged as the device layer number increases (Fig. 5(a) & (b)), thus limiting the increase in current carrying capability of the device. With such limitation on current injection into the MoS_2 channel, it is not meaningful to directly compare the "per-layer" current limit for such devices, because different layers do not necessarily carry the same share of electrical current (thus do not contribute equally to the overall current carrying ability of the multilayer devices). This limitation, however, may be removed if pure 1D edge contact[42] is used (Fig. 5(c) & (d)). Therefore, using edge contact in multilayer MoS_2 FETs shall enhance device performance by improving the current injection efficiency. Second, even for devices with pure edge contact (and each layer may carry and contribute the same amount of electrical current), multilayer devices

Nanoscale Accepted Manuscript

still have lower breakdown current values than single-layer devices do, because the efficiency of heat dissipation to the surrounding environment does not scale with the device thickness. It has been shown that heat dissipation to the substrate is the main cooling mechanism in substrate-supported graphene devices[29,43] (and we expect similar case in MoS_2 devices): while the thermal conductance may be lower at the layered material-substrate interface (compared to the in-plane value), the footprint area (length × width) of a device is usually orders-of-magnitude larger than its in-plane cross section area (thickness × width); this determines that the thermal conductance to the substrate dominates (Fig. 5(e)). As a result, while heat generation scales linearly with device layer number (assuming a constant current density), the device's thermal conductance to its surrounding does not increase proportionally (Fig. 5(f)). This causes the temperature of the device to rise more readily for thicker devices, and is responsible for their relatively lower "per-layer" current density (note that the total breakdown current is still higher) compared with thinner devices. Finally, for fair comparison between multilayer and single-layer devices, with normalized "per-layer" performance that would directly scale with the number of layers, both the following conditions are needed: (i) pure 1D edge contacts are ensured in both single-layer and multilayer devices, and (ii) substrate effects should be removed or made independent of device thickness. We illustrate, in Fig. 5 (g) & (h), that suspended MoS_2 FETs with 1D edge contacts will have both electrical conductance and thermal conductance scale linearly with number of layers (device thickness), in which performance can be normalized to "per-layer" measures. We note, however, removal of the substrate in suspended devices also eliminates the large-area, efficient heat dissipation pathway[44], thus suspended MoS_2 FETs (regardless of thickness) are expected to have earlier breakdown than their substrate-supported counterparts, and are hence undesirable for applications requiring higher electrical current and thermal budget.

Nanoscale Accepted Manuscript

To quantitatively understand the effect of device parameters on Joule heating, thermal dissipation, and consequently the current carrying limit, we perform FEM simulation to study the device breakdown current and voltage with varying MoS_2 channel thickness, length, and conductivity (Fig. 6). While our measurements are performed in air, where MoS_2 oxidation rate increases above 400°C, to study the ultimate device performance we model the process in vacuum: under Joule heating, MoS_2 temperature raises until reaching its melting temperature T_M (1458K), at which point the device breaks down (Fig. 6(a)). In the simulation we use MoS_2 thermal conductivity of 34.5W/(m·K)[45]. Consistent with the trend observed in experiments, our FEM results show that thicker MoS_2 devices breakdown at higher current (Fig. 6(b)), confirming that multilayer devices are better suited for applications that require high current. Longer device channel (large L value) leads to higher voltage and lower current at breakdown (Fig. 6(c)). The breakdown current can also be affected by the electrical conductivity (σ) of the MoS_2 channel: when σ increases, less Joule heating will be generated for a given current, resulting in higher breakdown current. In practice, both V_G and temperature can affect σ. Here, we show the σ dependence of I_{BD} and J_{BD} (Fig. 6(d)). We find both I_{BD} (Fig. 6(d)) and J_{BD} (inset) increases with σ. This suggests that improving device conductance is an effective approach to boost the current carrying and power handling capacity of MoS_2 transistors.

In summary, we have studied multilayer MoS_2 FETs and device performance dependence on parameters such as thickness. We have investigated the electrical breakdown of multilayer MoS_2 devices. Both experiments and FEM simulation show that multilayer MoS_2 transistors possess higher current-carrying capacities. Both experiments and analytic modeling show that multilayer devices exhibit higher mobility compared to mono- or few-layer devices, which contributes to the more conductive channel and higher current limit. Our results suggest that multilayer MoS_2

Nanoscale Accepted Manuscript

devices outperform their single- or few-layer counterparts in certain aspects, and their performance can be further improved by carefully engineering the devices and contacts.

Acknowledgement: We thank J. Lee, J. Shan, K. He, and I. Martin for helpful discussions and technical support, and Y. Wu for help with the illustration. We thank the support from Case School of Engineering, National Academy of Engineering (NAE) Grainger Foundation Frontier of Engineering (FOE) Award (FOE 2013-005), and Case Western Reserve University (CWRU) Provost's ACES+ Advance Opportunity Award.

Nanoscale Accepted Manuscript

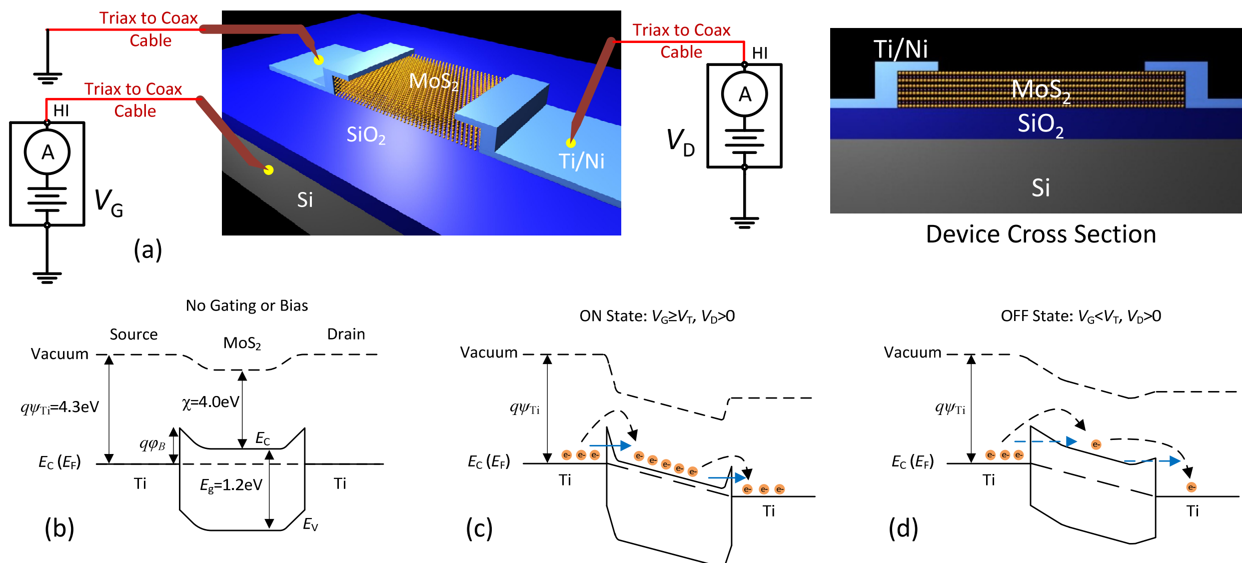

Fig. 1: Schematic of the device geometry, measurement setup, and working principle for multilayer MoS_2 FETs. (a) 3D illustration of a multilayer MoS_2 transistor with electrical connections, and cross-sectional view of the device. (b)-(d) Band diagrams of MoS_2 and contacting metal under different gate and drain biases, including (b) equilibrium, (c) ON state and (d) OFF state. *Blue arrows*: thermally assisted carrier tunneling. *Black arrows*: thermionic emission. Solid arrows indicate high-probability events, and dashed arrows show the opposite. All schematics are not drawn to scale.

Nanoscale Accepted Manuscript

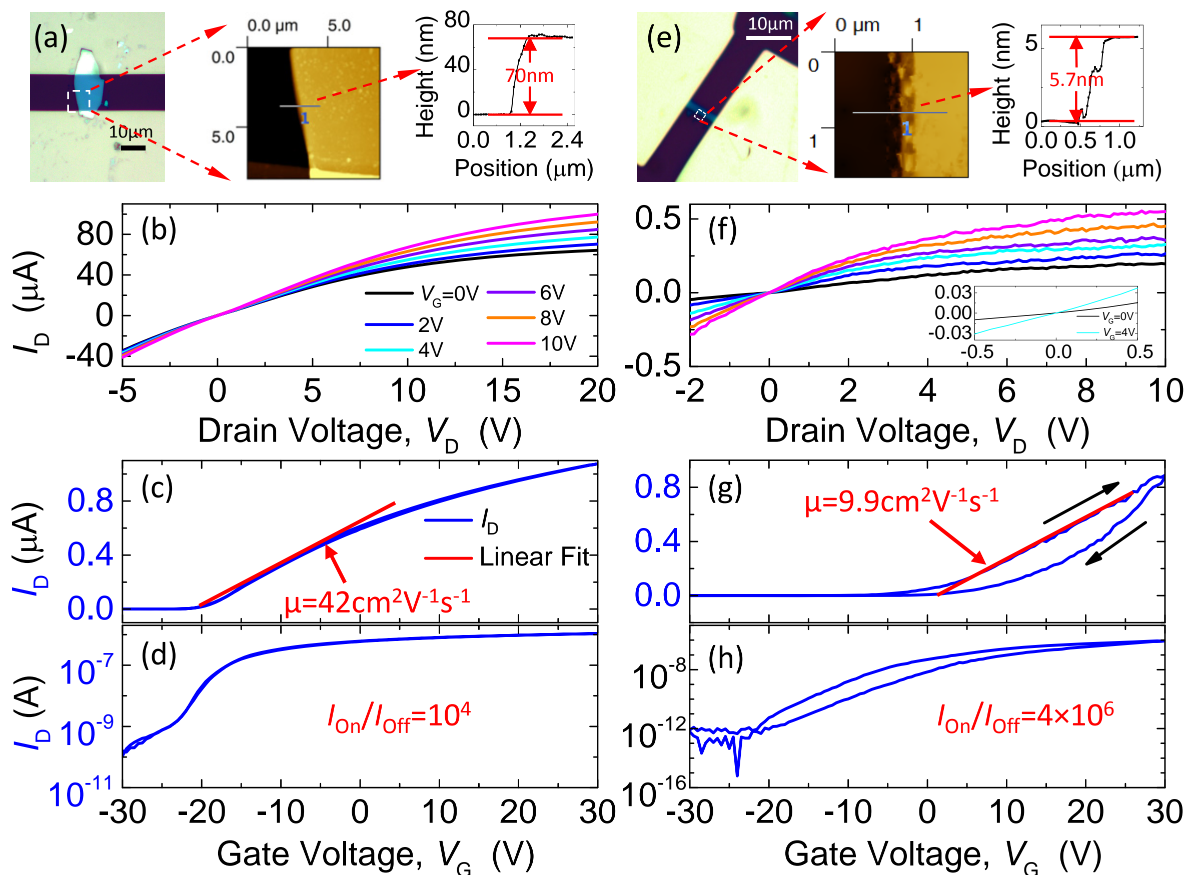

Fig. 2: (a)-(d) Measurement of MoS_2 device A (contact: 3nm Ti /50nm Ni). (a) Optical image, AFM image, and the height profile. (b) Transport characteristics. (c) & (d) Transfer curves in linear and logarithmic scales measured at V_D =0.1V. *Red line*: field-effect mobility extracted from the slope of the I_D-V_G curve. (e)-(h) Measurement of MoS_2 device B (contact: 2nm Ti /150nm Ni). The contents of the (e)-(h) are in the same sequence as in (a)-(d). Inset of (f) shows linear behavior at small V_D. Data in (g) is taken at V_D=1V.

Nanoscale Accepted Manuscript

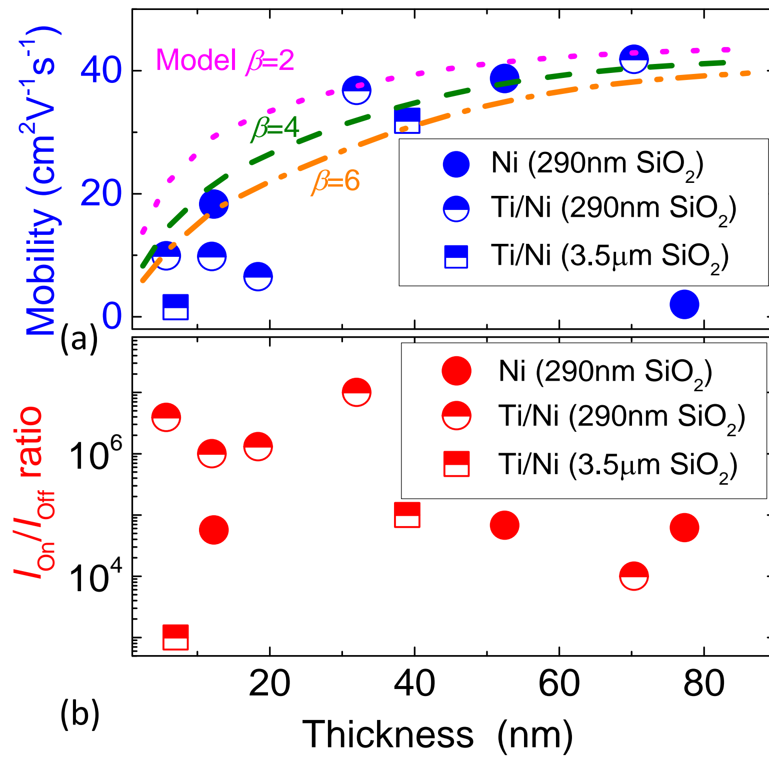

Fig. 3: Extracted (a) mobility, and (b) on/off ratio of devices with different MoS_2 thicknesses and with Ni (solid circles) and Ti/Ni contact (half-filled circles). Magenta, olive and orange lines in (a) show the calculated thickness dependence of mobility from multiple scattering terms with fitting parameters β=2, 4, and 6, respectively.

Nanoscale Accepted Manuscript

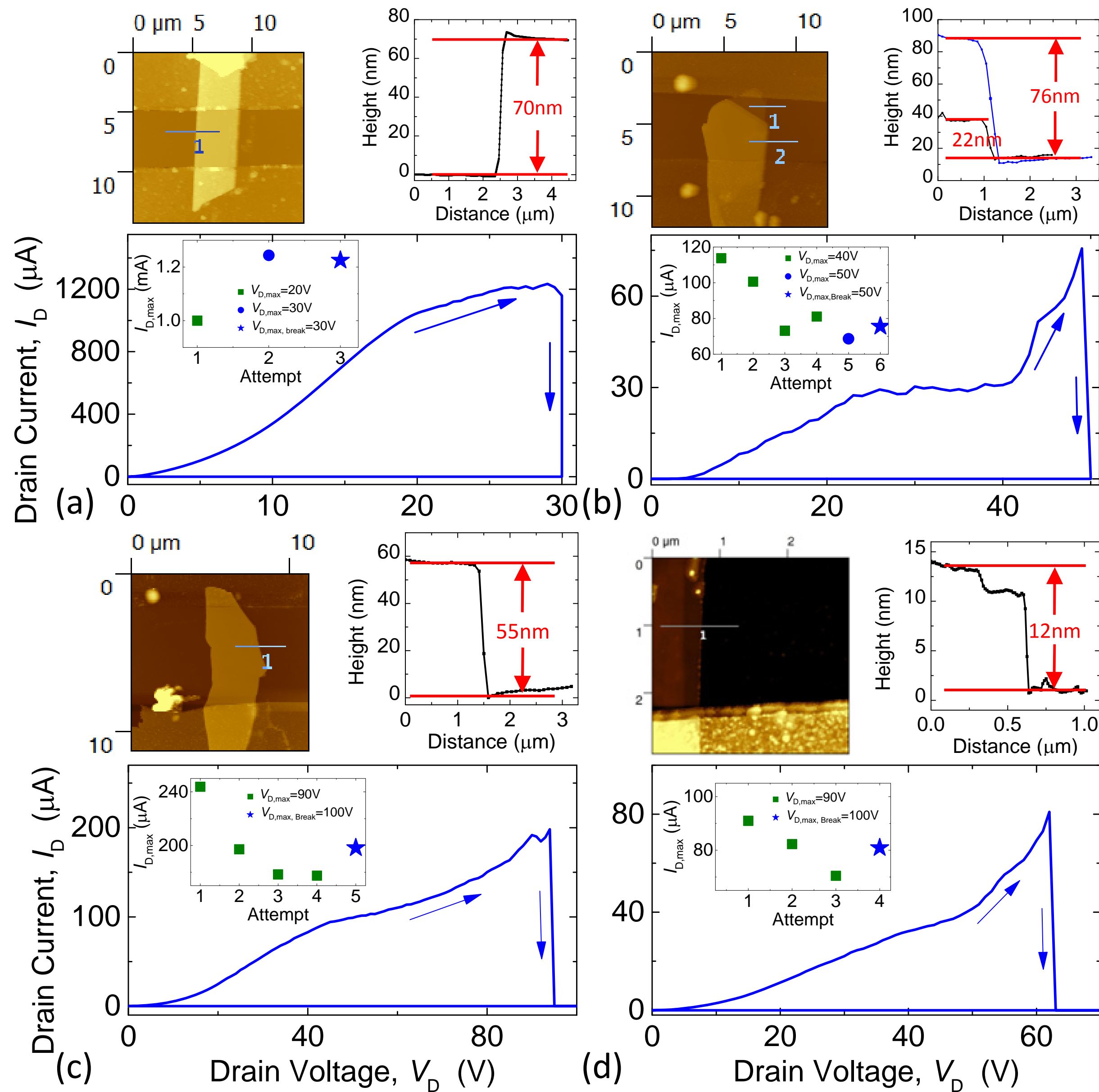

Fig. 4: Electrical breakdown of multilayer MoS_2 FETs. AFM images and height profiles are shown for all the devices. (a) I_D-V_D curve of a 70nm thick device, showing breakdown at I_D≈1.2mA. (b)-(d) Measurement of three other devices with different thicknesses. *Insets*: Maximum I_D in subsequent V_D sweeps with increasing ranges prior to breakdown.

Nanoscale Accepted Manuscript

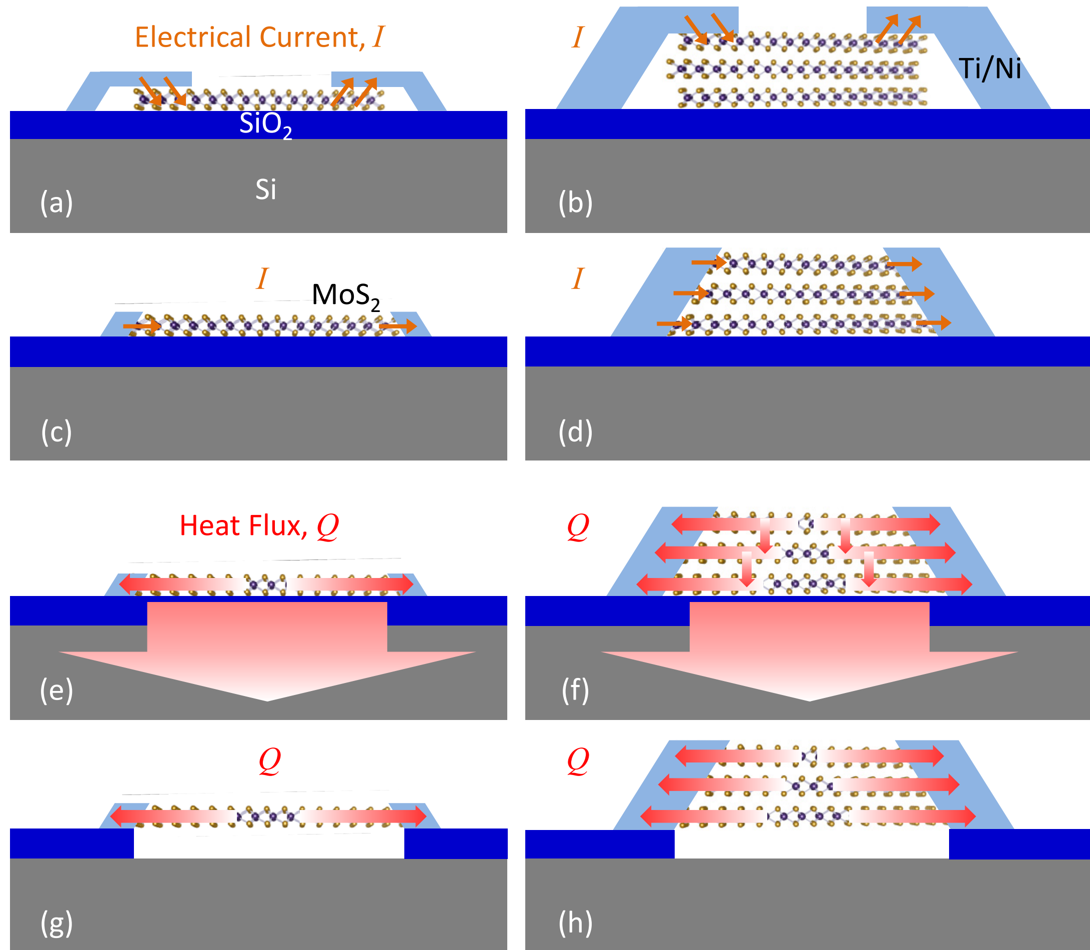

Fig. 5: Illustration of electrical current (a-d, orange arrows) and heat flux (e-h, red arrows) in single layer (a,c,e,g) and multilayer (b,d,f,h) MoS_2 FETs. (a) and (b) show the electrical current injection at 2D surface contacts to MoS_2 channels, while (c) and (d) show the scenario for 1D edge contacts. (e) and (f) illustrate heat flux in substrate-supported MoS_2 devices under Joule heating, while (g) and (h) show that in suspended MoS_2 channels.

Nanoscale Accepted Manuscript

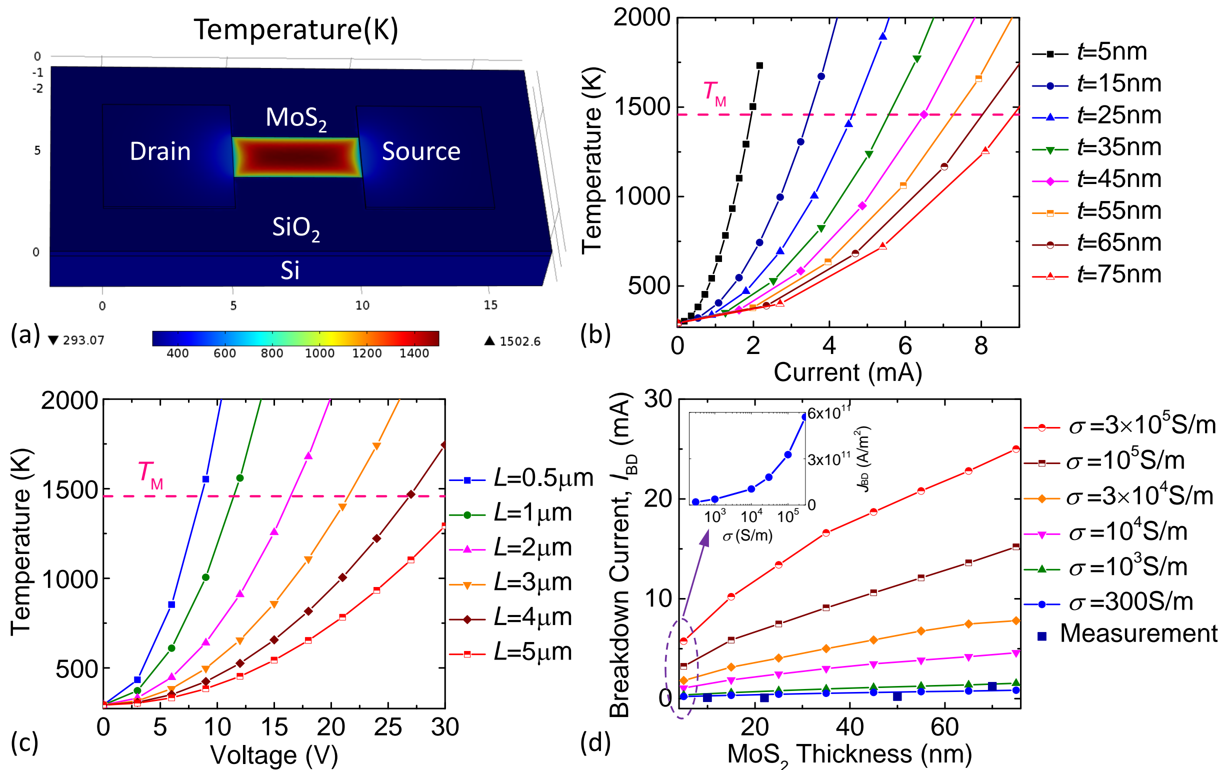

Fig. 6: FEM simulation of breakdown of MoS_2 transistors due to Joule heating. (a) Temperature profile of a 14.3kΩ FET with MoS_2 channel dimension t=5nm, L=5μm, W=2μm, with V_D=33V. Plotted in (b) & (c) is the maximum temperature in the MoS_2 channel, as a function of (b) I_D (for different MoS_2 thicknesses), and (c) V_D (for different channel lengths). *Horizontal dashed line*: T_M=1458K, the melting temperature of MoS_2. (d) I_{BD} as a function of MoS_2 thickness, for different channel conductivities. *Blue squares*: experimental data. *Inset*: J_{BD} as a function of MoS_2 conductivity for t=5nm devices.

Nanoscale Accepted Manuscript

References

[1] Q. H. Wang, K. Kalantar-Zadeh, A. Kis, J. N. Coleman, M. S. Strano, Nat. Nanotechnol. **7**, 699 (2012).

[2] Y. Yoon, K. Ganapathi, S. Salahuddin, Nano Lett. **11**, 3768 (2011).

[3] D. Jariwala, V. K. Sangwan, L. J. Lauhon, T. J. Marks, M. C. Hersam, ACS Nano **8**, 1102 (2014).

[4] B. Radisavljevic, A. Radenovic, J. Brivio, V. Giacometti, A. Kis, Nat. Nanotechnol. **6**, 147 (2011).

[5] B. Radisavljevic, A. Kis, Nat. Mater. **12**, 815 (2013).

[6] B. W. H. Baugher, H. O. H. Churchill, Y. Yang, P. Jarillo-Herrero, Nano Lett. **13**, 4212 (2013).

[7] H. Liu, M. Si, Y. Deng, A. T. Neal, Y. Du, S. Najmaei, P. M. Ajayan, J. Lou, P. D. Ye, ACS Nano **8**, 1031 (2014).

[8] H. Fang, M. Tosun, G. Seol, T. C. Chang, K. Takei, J. Guo, A Javey, Nano Lett. **13**, 1991 (2013).

[9] D. Fu, J. Zhou, S. Tongay, K. Liu, W. Fan, T.-J. K. Liu, J. Wu, Appl. Phys. Lett. **103**, 183105 (2013).

[10] J.-R. Chen, P. M. Odenthal, A. G. Swartz, G. C. Floyd, H. Wen, K. Y. Luo, R. K. Kawakami, Nano Lett. **13**, 3106-3110 (2013).

[11] I. Popov, G. Seifert, D. Tomanek, Phys. Rev. Lett. **108**, 156802 (2012).

[12] B. Radisavljevic, M. B. Whitwick, A. Kis, ACS Nano **5**, 9934 (2011).

[13] H. Wang, L. Yu, Y.-H. Lee, W. Fang, A. Hsu, P. Herring, M. Chin, M. Dubey, L.-J. Li, J. Kong, T. Palacios, IEEE Int. Electron Devices Meet., 4.6.1-4.6.4 (2012).

[14] H. Wang, L.Yu, Y.-H. Lee, Y. Shi, A. Hsu, M. L. Chin, L.-J. Li, M Dubey, J. Kong, T. Palacios, Nano Lett. **12**, 4674 (2012).

[15] M. S. Choi, G.-H. Lee, Y.-J. Yu, D.-Y. Lee, S. H. Lee, P. Kim, J. Hone, W. J. Yoo, Nat. Commun. **4**, 1624 (2013).

Nanoscale Accepted Manuscript

[16] H. Liu, A.T. Neal, P. D. Ye, ACS Nano **6**, 8563 (2012).

[17] H. Liu, P. D. Ye, IEEE Electron Device Lett. **33**, 546 (2012).

[18] S. Das, H.-Y. Chen, A. V. Penumatcha, J. Appenzeller, Nano Lett. **13**, 100 (2013).

[19] S. Kim, A. Konar, W.-S. Hwang, J. H. Lee, J. Lee, J. Yang, C. Jung, H. Kim, J.-B. Yoo, J.-Y. Choi, Y. W. Jin, S. Y. Lee, D. Jena, W. Choi, K. Kim, Nat. Commun. **3,** 1011 (2012).

[20] W. S. Hwang, M. Remskar, R. Yan, T. Kosel, J. K. Park, B. J. Cho, W. Haensch, H. Xing, A. Seabaugh, D. Jena, Appl. Phys. Lett. **102**, 043116 (2013).

[21] W. Liu, J. Kang, W. Cao, D. Sarkar, Y. Khatami, D. Jena, K. Banerjee, IEEE Int. Electron Devices Meet., 19.4.1-19.4.4 (2013).

[22] W. Bao, X. Cai, D. Kim, K. Sridhara, M. S. Fuhrer, Appl. Phys. Lett. **102**, 042104 (2013).

[23] H. Nam, S. Wi, H. Rokni, M. Chen, G. Priessnitz, W. Lu, X. Liang, ACS Nano **7**, 5870 (2013).

[24] S. Das, J. Appenzeller, Phys. Status Solidi Rapid Res. Lett. **7**, 268 (2013).

[25] H.-Y. Chang, S. Yang, J. Lee, L. Tao, W.-S. Hwang, D. Jena, N. Lu, D. Akinwande, ACS Nano **7**, 5446 (2013).

[26] J. Lee, H.-Y. Chang, T.-J. Ha, H. Li, R. S. Ruoff, A. Dodabalapur, D. Akinwande, IEEE Int. Electron Devices Meet., 19.2.1-19.2.4 (2013).

[27] D. J. Late, Y-K Huang, B. Liu, J. Acharya, S. N. Shirodkar, J. Luo, A. Yan, D. Charles, U. V. Waghmare, V. P. Dravid, C. N. R. Rao, ACS Nano **7**, 4879 (2013).

[28] Z. Tan, H. Tian, T. Feng, L. Zhao, D. Xie, Y. Yang, L. Xiao, J. Wang, T.-L. Ren, J. Xu, Appl. Phys. Lett. **103**, 263506 (2013).

[29] A. D. Liao, J. Z. Wu, X. Wang, K. Tahy, D. Jena, H. Dai, E. Pop, Phys. Rev. Lett. **106**, 256801 (2011).

[30] D. Lembke, A. Kis, ACS Nano **6**, 10070 (2012).

[31] D. Jariwala, V. K. Sangwan, D. J. Late, J. E. Johns, V. P. Dravid, T. J. Marks, L. J. Lauhon, M. C. Hersam, Appl. Phys. Lett. **102**, 173107 (2013).

[32] K. Kaasbjerg, K. S. Thygesen, K. W. Jacobsen, Phys. Rev. B **85**, 115317 (2012).

Nanoscale Accepted Manuscript

[33] M. Fuhrer, J. Hone, Nat. Nanotechnol. **8**, 1476 (2013).

[34] R. Ganatra, Q. Zhang, ACS Nano **8**, 4074 (2014).

[35] N. Ma, D. Jena, Phys. Rev. X **4**, 011043 (2014).

[36] S.-L. Li, K. Wakabayashi, Y. Xu, S. Nakaharai, K. Komatsu, W.-W. Li, Y.-F. Lin, A. Aparecido-Ferreira, K. Tsukagoshi, Nano Lett. **13**, 3546 (2013).

[37] B. L. Gelmont, M. Shur, M. Stroscio, J. Appl. Phys. **77**, 657 (1995).

[38] P. E. Hopkins, J. Appl. Phys. **105**, 093517 (2009).

[39] M. Ghorbani-Asl, A. N. Enyashin, A. Kuc, G. Seifert, T. Heine, Phys. Rev. B **88**, 245440 (2013).

[40] J.-H. Chen, W. G. Cullen, C. Jang, M. S. Fuhrer, E. D. Williams, Phys. Rev. Lett. **102**, 236805 (2009).

[41] Y. Tokura, T. Saku, Y. Horikoshi, Phys. Rev. B **53**, R10528 (1996).

[42] L. Wang, I. Meric, P. Y. Huang, Q. Gao, Y. Gao, H. Tran, T. Taniguchi, K. Watanabe, L. M. Campos, D. A. Muller, J. Guo, P. Kim, J. Hone, K. L. Shepard, C. R. Dean, A. R. H. Walker, H. G. Xing, Science **342**, 614 (2013).

[43] K. F. Mak, C. H. Lui, T. F. Heinz, Applied Physics Letters **97**, 221904 (2010).

[44] E. Pop, D. Mann, J. Cao, Q. Wang, K. Goodson, H. Dai, Phys. Rev. Lett. **95**, 155505 (2005).

[45] R. Yan, J. R. Simpson, S. Bertolazzi, J. Brivio, M. Watson, X. Wu, A. Kis, T. Luo, A. R. H. Walker, H. G. Xing, ACS Nano **8**, 989 (2014).

Nanoscale Accepted Manuscript